Effects of manganese incorporation on the morphology, structure and cytotoxicity of spherical bioactive glass nanoparticles

Breno R. Barrioni[1,*], Parichart Naruphontjirakul[2,3], Elizabeth Norris[3], Siwei Li[3], Nicole L. Kelly[4,5], John V. Hanna[5], Molly M. Stevens[3], Julian R. Jones[3] and Marivalda de M. Pereira[1]

[1] Department of Metallurgical Engineering and Materials, Federal University of Minas Gerais, School of Engineering, Belo Horizonte, MG, Brazil

[2] Biological Engineering Program, King Mongkut's University of Technology Thonburi, Thailand

[3] Department of Materials, Imperial College London, South Kensington, London, SW7 2AZ, UK

[4] MAS CDT, Senate House, University of Warwick, Coventry, CV4 7AL, UK

[5] Department of Physics, University of Warwick, Coventry CV4 7AL, UK

*Corresponding author. Tel.: +5531984764001

E-mail addresses: brenorb@ufmg.br (B. R. Barrioni); parichart.nar@kmutt.ac.th (P. Naruphontjirakul); e.norris14@imperial.ac.uk (E. Norris); siwei.li@imperial.ac.uk (S. Li); n.kelly.1@warwick.ac.uk (N. L. Kelly); j.v.hanna@warwick.ac.uk (J. V. Hanna); m.stevens@imperial.ac.uk (M. M. Stevens); julian.r.jones@imperial.ac.uk (J. R. Jones); mpereira@demet.ufmg.br (M. M. Pereira)

Abstract Bioactive glass nanoparticles (BGNPs) are of great interest in tissue engineering as they possess high dissolution rate and capability of being internalized by cells, releasing their dissolution products with therapeutic benefits intracellularly. A modified Stöber process can be applied to obtain different BGNPs compositions containing therapeutic ions while maintaining controllable particle morphology, monodispersity and reduce agglomeration. Here, BGNPs containing Mn, an ion that has been shown to influence the osteoblast proliferation and bone mineralization, were evaluated. Particles with up to 142.3 ± 10.8 nm and spherical morphology were obtained after MnO incorporation in the SiO_2 – CaO system. X-ray photoelectron spectroscopy (XPS) indicated the presence of Mn^{2+} species and also a reduction in the number of bridging oxygen bonds due to the Ca and Mn. The Ca and Mn network modifier role on the silica network was also confirmed by magic-angle spinning ^{29}Si solid-state nuclear magnetic resonance (MAS NMR). MTT evaluation showed no reduction in the mitochondrial metabolic activity of human mesenchymal stem cells exposed to the glass ionic products. Thus, evaluation showed that Mn could be incorporated into BGNPs by the modified Stöber method while maintaining their spherical morphology and features as a promising strategy for tissue regeneration.

Keywords: bioactive glass, manganese, nanoparticles, Stöber

1 Introduction

Bioactive glasses (BGs) are potential materials for tissue engineering due to their ability to bond with bone [1], their controlled degradability and capacity to stimulate new tissue formation [2,3]. BGs can be produced by the sol-gel method, in which materials with a higher compositional range of bioactivity, higher surface area and nanoporosity can be obtained, resulting in improved binding to the living tissues when compared to melt-derived glasses with the same composition [4]. The sol-gel synthesis also allows the incorporation of different ions with therapeutic properties into the silica network that can be released during the dissolution process, enhancing their properties. Each component has a specific role on the BG functionality, such as influencing angiogenesis (copper), treating osteoporosis (strontium) or stimulating new bone formation (magnesium), among others [5]. The use of these ions are of great interest in tissue engineering strategies, improving the bioactive glass performance, but the effect of the incorporation of each ion on the glass structure must be evaluated.

Bioactive glass nanoparticles (BGNPs) present advantages over microparticles, such as high surface to volume ratio, increasing the dissolution rate and also improving the interactions with other materials or biomolecules [6]. These nanoparticles can be internalized into cells, accumulating inside the lysosome, and releasing its dissolution products with therapeutic benefits intracellularly [7,8], and are considered for different application in tissue regeneration, such as injectable biomaterials and nanocomposites synthesis. Previous work showed that BGNPs of up to 215 ± 20 nm can be internalized by different types of cells, such as human bone marrow and adipose-derived stem cells, releasing the dissolution products inside the cells [7,9]. Spherical silica particles in a wide size range and controlled particle size can be obtained by the Stöber process [10]. In this sol-gel based method, a silicon alkoxide precursor, such as TEOS (tetraethoxysilane), is hydrolysed in an ammonia-catalysed process followed by polycondensation and Si-O-Si bond formation, resulting in a dispersed nanoparticles suspension. Spherical and monodispersed silica nanoparticles are formed due to the repulsive forces between the particles, as a result of $Si\text{-}OH^-$ formation under basic conditions [8]. By controlling the reaction parameters it is possible to obtain particles with different sizes, distribution and morphology. For example, by altering the ammonia concentration, silica particles from 10 to 500 nm can be synthesized [11], and particle size tend to reduce along with the ammonia concentration [8]. However, the incorporation of network modifier ions on the silica network may lead to the particles becoming irregular, and adjusting the process variables is necessary to preserve the

particles monodispersity and reduce agglomeration [8,12]. Nonetheless, an effective way to incorporate calcium on silica nanoparticles was described by Greasley et al., using a modified Stöber procedure to obtain nanoparticles on the binary bioactive glass system SiO_2 – CaO [8], that have been shown great bioactivity [13,14]. However, a maximum of 10 mol% CaO was incorporated [8].

Among different ions that could be incorporated into the bioactive glass network, manganese (Mn) has been shown to influence biological activities such as extracellular matrix remodelling [15] and bone mineralization [16]. This ion was previously incorporated into bioceramics such as tricalcium phosphate, improving the bone mineralization rate, although it has also shown that the Mn concentration should be properly adjusted [16]. Higher cell adhesion potential was also observed on Mn-containing hydroxyapatites when compared to the pure hydroxyapatite [17]. Melt-derived bioactive glasses containing Mn presented a good degree of bioactivity and no cytotoxic effects on human MG-63 osteoblasts cultured up to 5 days. Mn-doped glasses also increased osteoblast proliferation and spreading capability, expression of alkaline phosphatase (ALP) and bone morphogenetic proteins [18]. Mn was also recently incorporated into mesoporous bioactive glass nanoparticles [19], resulting in a multifunctional nanoparticle for bone tissue engineering. Nonetheless, a rapid Si, Ca, P and Mn ion release was observed during the dissolution study in the cell culture medium. High dissolution rates may lead to critical ion concentration levels, influencing cell function, expression and gene metabolism [20]. Therefore, nanoparticles with controlled ion release are desired, and dense nanoparticles can be a promising alternative for therapeutic ion release strategies.

The combination of nanotechnology approaches with the therapeutic properties of ions released from the BGs is an attractive strategy for the development of materials with improved properties for tissue regeneration. Here, the aim was to incorporate Mn into dense spherical BGNPs and to evaluate the effect of Mn incorporation on the glass composition, structure, morphology, controlled ion release capability and cytotoxicity.

2 Materials and Methods

2.1 Synthesis of bioactive glass

Bioactive glass nanoparticles were obtained using the modified Stöber method [8,12]. In this procedure, ethanol absolute (ethyl alcohol, 99.5 %, *VWR*, UK), distilled water and ammonium hydroxide (NH_4OH, 28 – 30 % NH_3 basis, *Sigma-Aldrich,* UK) were

mixed using a magnetic stirrer for 10 minutes. Then, TEOS (98%, *Sigma-Aldrich*, UK) was slowly mixed with the solution, and the magnetic stirring was left overnight. After that, SiO_2 nanoparticles were collected by centrifugation at 7830 rpm for 40 minutes and washed three times with ethanol. Concentrations of 0.28 M TEOS, 0.23 M NH_4OH and 6 M H_2O were used. Samples were dried for 24 h at 60 °C.

Control silica samples (NP-R) were obtained after thermal treatment at 680 °C, for 3 h, on a heating rate of 3 °C.min^{-1}. Samples in the SiO_2 – CaO system were produced at 1 Si : 1.3 Ca molar ratio, in accordance with previous work, in which this ratio was found to be optimal for maximum calcium incorporation [8]. The dried silica particles were dispersed in water and mixed with a solution containing calcium nitrate tetrahydrate (99%, *Acros Organics,* UK) in the ultrasonic bath for 30 minutes. Then, the solution was centrifuged to collect the particles, samples were dried at 60 °C for 24 h and then thermally treated at 680 °C, for 3 h, at 3 °C.min^{-1} heating rate. After thermal treatment, particles were washed three times with ethanol to remove the excess of ions that were not incorporated into the glass network. The SiO_2 – CaO sample was named NP-100Ca.

Mn was incorporated into the glass network by partial replacement of the Ca content to obtain particles in the SiO_2 – CaO – MnO system. Two samples were obtained, with 25 % substitution (NP-25Mn, Si : Ca : Mn molar ratio of 1 : 0.98 : 0.35) and 50 % substitution (NP-50Mn, Si : Ca : Mn molar ratio of 1 : 0.65 : 0.65). For that, solutions containing calcium nitrate tetrahydrate and manganese nitrate hydrate (98%, *Sigma-Aldrich*, UK) were prepared and the same process described before for calcium incorporation was applied.

2.2 Characterization of bioactive glass nanoparticles

Chemical composition

To evaluate the chemical compositions of the obtained BGNPs, the acid digestion method was performed. In a platinum crucible, a total of 250 mg of anhydrous lithium metaborate (80% w/w) and lithium tetraborate (20% w/w) (*Spectroflux 100B*, Alfa Aesar, UK) was mixed with 50 mg of each sample. The mixture was then fused at 1050 °C for 30 minutes. After cooling, samples were completely dissolved in nitric acid 2M (HNO_3, *VWR*, UK), and the concentrations of Si, Ca and Mn in each sample were determined by inductively coupled plasma-optical emission spectrometer (ICP-OES; Thermo Scientific iCaP 6000series equipment, USA), and the proportions of SiO_2, CaO, and MnO were calculated.

Morphological and textural properties

Particle size was determined using dynamic light scattering (DLS, Malvern Instrument 2000) and to confirm size and morphology, a JEOL 2100 Plus transmission electron microscopy (TEM) was used operating at 200 kV. Before DLS and TEM analysis, samples were dispersed in ethanol absolute in an ultrasonic bath for 15 minutes. For TEM analysis, particles dispersed in ethanol absolute were collected on a copper grid (400 mesh) coated with a carbon film (*TAAB*, UK). Zeta potential was performed on a Zetasizer Malvern Instrument 2000, in order to evaluate the particles stability in solution. Samples were dispersed in distilled water before zeta potential measurements.

Nitrogen sorption was performed in a Quantachrome Autosorb AS-6 multi-station with 40 absorption points and 40 desorption points. Samples were degassed for 24 h at 200 °C prior to measurement. To evaluate the surface area of samples the Brunauer-Emmett-Teller (BET) method was applied [21], and absorption data points in the range of 0.01 – 0.30 (P/P_0) relative pressure were used, whereas the pore diameter distribution was evaluated by the Barret-Joyner-Halenda (BJH) method [22] applied to the desorption curves.

Structural evaluation

Fourier transform infrared spectroscopy (FTIR) was performed on a Thermo Scientific Nicolet iS10 equipment equipped with the Attenuated Total Reflectance (ATR) Accessory. Spectra were obtained in the range of 400 to 4000 cm^{-1} (4 cm^{-1} resolution; 32 scans per spectrum). X-ray diffraction (XRD) patterns were obtained on a Bruker D2 desktop, with 0.02° step size and a CuKα radiation source. The diffraction data were collected from 7 to 70° (2θ). X-ray photoelectron spectroscopy (XPS) analysis was conducted on a Thermo Scientific K-Alpha$^+$ system, operating at a base pressure of 2 x 10^{-9} mbar. A monochromated and microfused Al Kα X-ray source (hv = 1486.6 eV) was incorporated to the system, with a 180° double focusing hemispherical analyser containing a 2D detector. A 6 mA emission current of the X-ray source and 12 kV anode bias was used. A flood gun was applied to minimize sample charging, and the remaining small shifts observed in the binding energy (BE) due to sample charging were corrected using as reference the C 1s core line, shifted to the binding energy of 285.0 eV. Surveys were obtained using X-ray spot size of 400 µm and 200 eV pass energy, whereas for core level scan a 20 eV pass energy was applied. Survey analysis was carried out to verify the glasses elemental compositions, and high-resolution core-

level scans were performed for Si 2p, O 1s, Ca 2p and Mn 2p. Data were evaluated using the Avantage XPS software package.

To evaluate the effect of Ca and Mn incorporation on the silica network, magic angle spinning ^{29}Si solid-state nuclear magnetic resonance (MAS NMR) measurements were performed on the BGs. All ^{29}Si single pulse MAS NMR measurements were performed at 7.05 T using a Varian/Chemagnetics InfinityPlus spectrometer operating at a ^{29}Si Larmor frequency (ν_o) of 59.6 MHz. These experiments were performed using a Bruker 7 mm HX probe which enabled a MAS frequency of 5 kHz to be implemented. Pulse length calibration was performed on solid kaolinite ($Al_2O_3 \cdot 2SiO_2 \cdot 2H_2O$) from which a π/2 pulse time of 4.25 μs was measured. All single-pulse measurements were undertaken with a π/2 nutation angle together with a recycle delay of 240 s. For the ^{29}Si single MAS pulse experiments, strong heteronuclear ^{1}H decoupling (100 kHz in strength) was applied. All ^{29}Si chemical shifts were externally referenced against the IUPAC recommended primary reference of Me_4Si (1 % in $CDCl_3$, δ_{iso} = 0.0 ppm), via the secondary solid kaolinite reference (δ_{iso} = −92 ppm) [22]. The degree of condensation (D_c) was calculated accordingly with the Eq. 1 [23].

$$D_c = (Q^1\% + 2 * Q^2\% + 3 * Q^3\% + 4* Q^4\%) / 4 \qquad \text{(Eq. 1)}$$

To obtain the bridging oxygen (BO) fraction from the Q-species the following contributions were considered: species Q^0, Q^1, Q^2, Q^3 and Q^4 contribute with respectively 0.0, 0.5, 1.0, 1.5 and 2.0 BO atoms per Si center and respectively 4.0, 3.5, 3.0, 2.5 and 2.0 total oxygen. The non-bridging oxygen (NBO) fraction was calculated by NBO = 1.0 – BO [24].

Ion release study

Samples were immersed in Dulbecco's Modified Eagle's medium (DMEM, *Gibco*, UK) at a glass to media ratio of 1.5 mg.mL^{-1} [7,25], to evaluate the ion dissolution rate. The particles were suspended in DMEM and placed in SnakeSkin Dialysis Tubing (3.5 K MWCO, 16 mm dry I.D; *ThermoFisher Scientific,* UK), then immersed in an airtight polyethylene container containing the solution to a final volume of 45 mL. Samples were placed on an incubator at 37 °C with an orbital shaker at 120 rpm. Aliquots of 1 mL were collected after 4, 8, 24, 48 and 72 h to evaluate the ionic concentration of the media, and then replaced with fresh 1 mL DMEM. The collected solutions were dissolved in 2 M HNO_3 solution, and the concentration of Si, Ca and Mn were measured by ICP-OES. Samples were run in triplicate. A DMEM solution alone was also incubated as described before to the other samples and used as a control.

2.3 Cytotoxicity study

To evaluate the effect of the glass ionic release product and Mn incorporation on the cell cytotoxicity, samples were soaked in a plain α-MEM (Modified Eagle's medium, *Gibco*, UK) with continuous agitation (120 rpm), at a concentration of 250 $\mu g.mL^{-1}$, according to previous studies [7]. After three days, the medium was centrifuged and the supernatant containing the ionic release product was collected. Human bone marrow-derived mesenchymal stem cells, hMSCs (ATCC® PCS-500-012™), were expanded in T-125 cell culture flasks (Corning®; *Sigma-Aldrich*, UK) in basal condition α-MEM supplement with 10% v/v foetal bovine serum (FBS), 100 $U.mL^{-1}$ penicillin and 100 $\mu g.mL^{-1}$ streptomycin (Gibco; *ThermoFisher Scientific*, UK) at 37°C, 5 $\%CO_2$ and fully humidified atmosphere. Passage 2 and 3 of the hMSCs were used for all studies at a concentration of 5×10^4 cells.mL^{-1}. The hMSC were treated for 2, 4 and 7 days with the ionic product media. Cell viability was determined by MTT, a colourimetric assay based on the conversion of 3-(4,5-dimethylthiazol-2-yl)-2,5-diphenyltetrazolium bromide into formazan (Invitrogen, Molecular ProbesTM, UK). Cells cultured on tissue culture plate (TCP) in plain α-MEM were used as control.

2.4 Statistical analysis

The chemical composition analysis, textural properties and ionic dissolution in DMEM experiments were performed in triplicate, and results are shown as mean ± standard deviation. MTT cell viability data are expressed as mean ± SD of three independent experiments (n = 3), and results were deemed significant if $p < 0.05$ (Kruskall-Wallis followed by Dunn's post test).

3 Results and Discussion

Compositional analysis

BGNPs were obtained using the Stöber method, incorporating Mn in partial replacement for the Ca content. Previous work has shown an optimal ratio of 1.3:1 Ca:Si for BGNPs synthesis, with no further increase on the Ca incorporation into the glass network when higher concentrations were used [8]. Therefore, this ratio was maintained for the synthesis of NP-100Ca, and calcium content was partially substituted by manganese for samples NP-25Mn (25 % substitution) and NP-50Mn (50

% substitution). For comparison purposes, SiO_2 reference nanoparticles were also related in this work (NP-R).

The amount of CaO in NP-100Ca (Table 1) was found to be 8.0 ± 1.2 mol %, which agreed with previous work at the same nominal Si:Ca ratio [8]. Calcium and manganese precursors were only added after the silica nanoparticle was formed, and they should deposit on the particle surface during drying, diffusing into the glass network at the final thermal treatment [8,26]. The excess of calcium and manganese not incorporated into the glass network was removed during the final washing step, a process that previously works showed to be essential on the bioactive glass nanoparticle synthesis, avoiding the formation of Mn and Ca-rich phases around the particles [8].

Table 1 also shows the average particle size measured by DLS, with diameter increasing after incorporation of ions. Previous work reported that particles with an average diameter below 250 nm can be internalized by cells, such as human bone marrow cells (MSCs) for local sustained delivery of therapeutic ions [9], which fits within the particle size range observed here (99-140 nm). The BGNPs displayed surfaces with a relatively high negative charge, ranging from -22 to -36 mV, which may be related to hydroxyl groups present on their surfaces [6]. Previous work showed that the attachment and proliferation of biomolecules and cells on the nanoparticles are improved when the zeta potential is negative [27,28]. Furthermore, nanoparticles with low zeta potential values, usually in the range of 5 and -5 mV, tend to coagulate or flocculate [28], whereas good stability is provided when zeta potential is around 30 mV (negative or positive) [29] and is desired for therapeutic nanoparticles.

Table 1: Measured composition of bioactive glass nanoparticles (mol%), determined by lithium metaborate fusion and ICP-OES, particle size distribution (DLS), zeta potential in DI water and specific surface area from nitrogen sorption evaluation via the BET method.

Samples	Measured composition (mol%)			Particle size (nm)	Zeta potential (mV)	Specific surface area ($m^2.g^{-1}$)
	SiO_2	CaO	MnO			
NP-R	100.0 ± 0.2	-	-	99.8 ± 10.2	-36.3 ± 0.6	42.9 ± 1.7
NP-100Ca	92.0 ± 1.1	8.0 ± 1.2	0 ± 0	112.1 ± 13.5	-35.1 ± 1.9	39.8 ± 0.7

NP-25Mn	93.8 ± 0.4	2.9 ± 0.2	3.3 ± 0.3	142.3 ± 10.8	-22.1 ± 0.2	35.9 ± 3.1
NP-50Mn	93.5 ± 0.3	2.3 ± 0.4	4.2 ± 0.2	139.6 ± 8.9	-23.9 ± 1.0	40.2 ± 1.1

Morphological and textural evaluation

Spherical nanoparticles were obtained, as shown by TEM (Figure 1). No remaining salt was observed, indicating that the washing step was efficient to remove the unincorporated Ca and Mn of the particle surface, and also avoiding agglomeration [12]. The morphology of the particles was similar to previously observed for materials obtained by this method [8,12], and the Mn content did not influence the spherical morphology, although at high magnification, changes in contrast became more apparent as Mn content increased (Figure 1(e)).

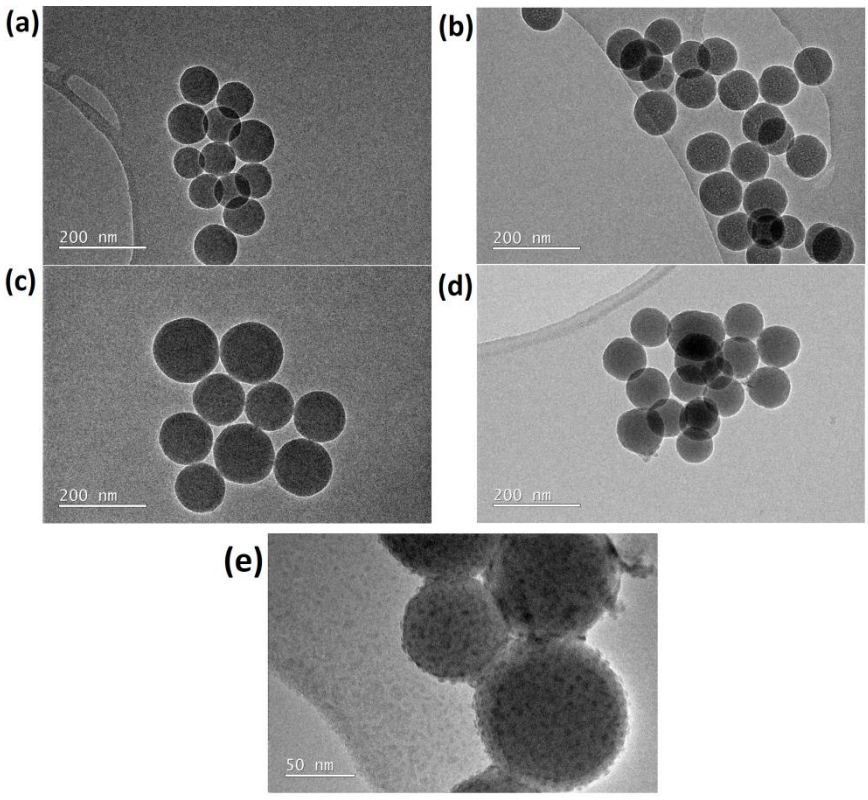

Figure 1: Bright field TEM images of (a) NP-R, (b) NP-100Ca, (c) NP-25Mn and (d) NP-50Mn and (e) higher TEM magnification of NP-50Mn. Scale bars = 200 nm (a-d) and 50 nm (e).

Specific surface areas between 35 and 43 m^2 g^{-1} were determined by BET (Table 1), which in the range expected for non-porous silica particles made in this way [30], with Mn content having little effect. Applying the BJH method to the desorption isotherm produced a pore size distribution, giving a modal diameter of ~24 nm, however the

pores were not visible in TEM and the value is likely to be generated from spaces between packed particles in the sample tube.

Structural characterization

Characteristic FTIR absorption bands of bioactive glasses were observed (Figure 2a) The broad band located between 1000 and 1300 cm^{-1} is often assigned to the Si-O-Si asymmetric stretching vibration [31,32], whereas the symmetric Si-O-Si stretching is observed at 800 cm^{-1} [31]. The bending mode of Si-O groups is assigned to the absorbance around 450 cm^{-1} [33] and is typical of Si-O in amorphous structures [34]. XRD patterns (Figure 2b) showed only a broad halo for all samples, typical of amorphous glass structures [33], with no qualitative difference between the different samples. No crystalline phases were observed in spite of calcium and manganese incorporation in the silica network and amorphous glass was maintained.

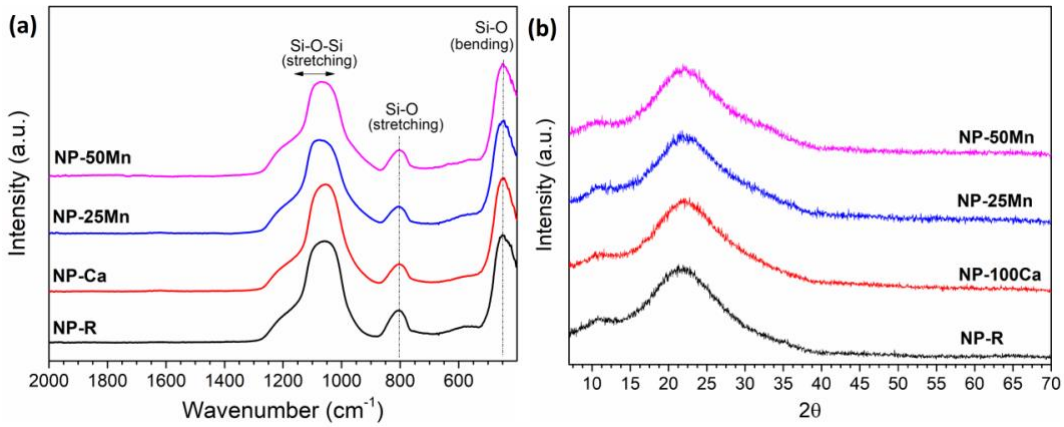

Figure 2: (a) FTIR spectra and (b) XRD patterns of bioactive glass nanoparticles.

Wide XPS scans for all samples are shown in Figure 3. It is possible to identify typical XPS and Auger lines from the particle constituent elements and also the C 1s peak, which is assigned to hydrocarbon impurities that can be absorbed by the glass surface [32]. The C 1s or “adventitious carbon” peak is used as a reference in XPS analysis, and the BE calibration was performed by setting this peak at 285.0 eV for sample charging correction.

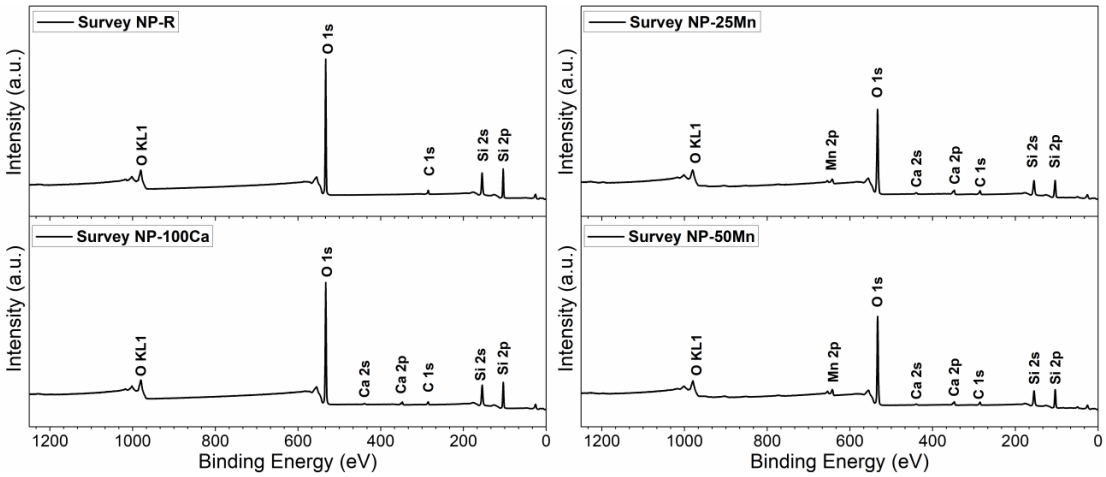

Figure 3: XPS wide scan spectra of BGNPs.

The semi-quantitative chemical composition of BGNPs surface was evaluated by XPS, and results expressed in atomic percentage are shown in Table 2. A high amount of C found on the glass surface can be related to hydrocarbonaceous impurities from the glass surface [32]. Mn and Ca at different concentrations were observed for NP-25Mn and NP-50Mn. The surface composition evaluated by XPS was also compared with the bulk composition previously investigated by ICP-OES, and the Si:Ca and Si:Mn atomic percentage ratios were calculated to evidence the Ca and Mn distribution from the surface to the inner core of the particles. Results show that Ca and Mn were not uniformly incorporated into the NP-25Mn and NP-50Mn particles, as higher concentration of those ions were observed on the surface when compared to the bulk. Ions were incorporated into the silica nanoparticles by the diffusion mechanism during thermal processing, which may cause inhomogeneity on the Mn and Ca distribution, allowing greater ionic concentration near the glass surface. However, losses due to the washing step may also remove network modifier cations from the surface. NP-100Ca presented similar glass surface and bulk atomic composition, which can be indicative of Ca migration throughout the entire particle. In fact, previous work has shown that SiO_2-CaO particles, with similar compositions to those prepared in this work, also presented homogeneous Ca distribution [8]. Although chemical composition inhomogeneity is usually observed in sol-gel glasses [26], the short diffusion distance for nanoparticles allows improved penetration of cations throughout the particles. However, this homogeneous diffusion profile was inhibited on samples containing both Mn and Ca.

Table 2: Chemical analysis obtained from XPS wide scan (%at) and calculated atomic ratio (Si:Ca and Si:Mn) based on XPS wide scan spectra and ICP-OES analysis.

Samples	XPS Chemical Analysis (%at)	XPS	ICP-OES

	Si 2p	O 1s	C 1s	Ca 2p	Mn 2p	Si:Ca ratio	Si:Mn ratio	Si:Ca ratio	Si:Mn ratio
NP-R	36.6	57.7	5.7	-	-	-	-	-	-
NP-100Ca	36.5	58	4.4	1.1	-	1:0.03	-	1:0.03	-
NP-25Mn	33.1	56.3	7.4	2.0	1.2	1:0.06	1:0.04	1:0.03	1:0.03
NP-50Mn	33.5	57.4	6.0	1.6	1.6	1:0.05	1:0.05	1:0.02	1:0.04

Figure 4a shows the high-resolution Si 2p core level. The NP-R Si 2p peak is narrower than that observed for other samples and slightly shifted to higher binding energies, which could be related to changes on the proportion of different silicate species formed on the glass network after Mn and Ca incorporation [24]. In silicate glasses, the oxygen that bonds two Si atoms together (Si-O-Si) is named bridging oxygen (BO), whereas it is non-bridging oxygen (NBO) when it is bonding Si atoms to a metal cation [35]. Q^n species are formed on the silica tetrahedral structure, in which *n* represents the number of BO bonds [36]. The incorporation of modifier ions disrupts the silica network, replacing BO units by NBO, and consequently changing the proportion of Q^n species present in the glass. The electron density over each Si atom should be different depending on the number of BO or NBO bonded to it, consequently shifting the BE for different Q^n species [24]. Lower values of BE are observed for structures containing higher NBO content [24], therefore the Si 2p core level evaluation indicates that the incorporated ions may be acting as network modifiers in the glass structure, replacing BO bonds by NBO structures. Nonetheless, the quantification of Q^n species is not trivial using these unresolved spectra. The O 1s spectra (Figure 4b) showed similar behaviour to that of Si 2p spectra, and a symmetric peak was observed at 533.1 eV for NP-R, whereas for other samples the peak maxima slightly shifted toward lower values of BE, and a broader peak was formed, with a more evident tail formed at lower energies. This could be indicative of an increased number of NBO structures due to the incorporation of Mn and Ca in the glass network. In fact, previous work showed that the O 1s BO signal is located at higher BE than NBO contributions in silicate glasses [24,35,37], indicating that the incorporation of ions into the glass may be disrupting the silica network, forming non-bridging structures, in accordance to the observed in the Si

2p evaluation. Furthermore, at higher BE values, the contribution of surface hydroxyls can also be present [38]. However, quantification of the BO and NBO units were not performed in this work, as the two components were not well resolved after deconvolution of the O 1s spectra, which could lead to inaccuracy of the relative areas and proportion of the different species [39].

No major difference was observed between the Ca 2p XPS spectra of different samples, as shown in Figure 4c. The typical and well-distinguished pairs from spin-orbit spitting, Ca $2p_{3/2}$ and Ca $2p_{1/2}$ [40], were observed in all samples around 347.8 eV and 351.3 eV, respectively, in accordance to the observed elsewhere for calcium compounds [41]. Furthermore, the Ca 2p spin-orbit spitting is usually around 3.5 eV for different compounds [41,42] and is in accordance with the results found in this work, indicating no difference between the calcium chemical environments for the different samples. Figure 4d presents the Mn 2p photoelectron lines for NP-25Mn and NP-50Mn, in which a doublet peak is observed due to typical Mn $2p_{3/2}$ and Mn $2p_{1/2}$ spin-orbit splitting [43]. The presence of a satellite peak can also be observed at a binding energy of around 4 eV higher than the main peak and is often related to the shake-up mechanism [44]. The identification of the different species contributing to the Mn 2p XPS spectra is difficult as this element has six stable oxidation states, some of them showing significant multiplet splitting and also overlapping binging energy ranges [45,46]. However, the binding energy values obtained is in the range of different Mn compounds reported in the literature [43,45,47]. Furthermore, the satellite peak observed at a higher binding energy of the Mn $2p_{3/2}$ peak is typical of the Mn^{2+} state, which could indicate the presence on manganese mainly as Mn^{2+} on the bioactive glass structure [48]. Indeed, previous reports have shown that higher Mn oxidation states, such as +4 and +7, are very unlikely in silicate systems, and this ion is usually present as Mn^{2+} when incorporated in silicate structures, although Mn^{3+} can also be observed, shifting the Mn $2p_{3/2}$ to higher values [49]. The shape and position of the Mn 2p spectra for both samples are similar, indicating that the Mn environment was maintained, although the intensity of these peaks can increase due to the higher Mn content [48]. XPS evaluation, therefore, indicated that Mn is in the glass network mainly in the Mn^{2+} state, acting as a network modifier on the glass structure, with the same structural role of calcium, reducing the number of BO and consequently the network connectivity.

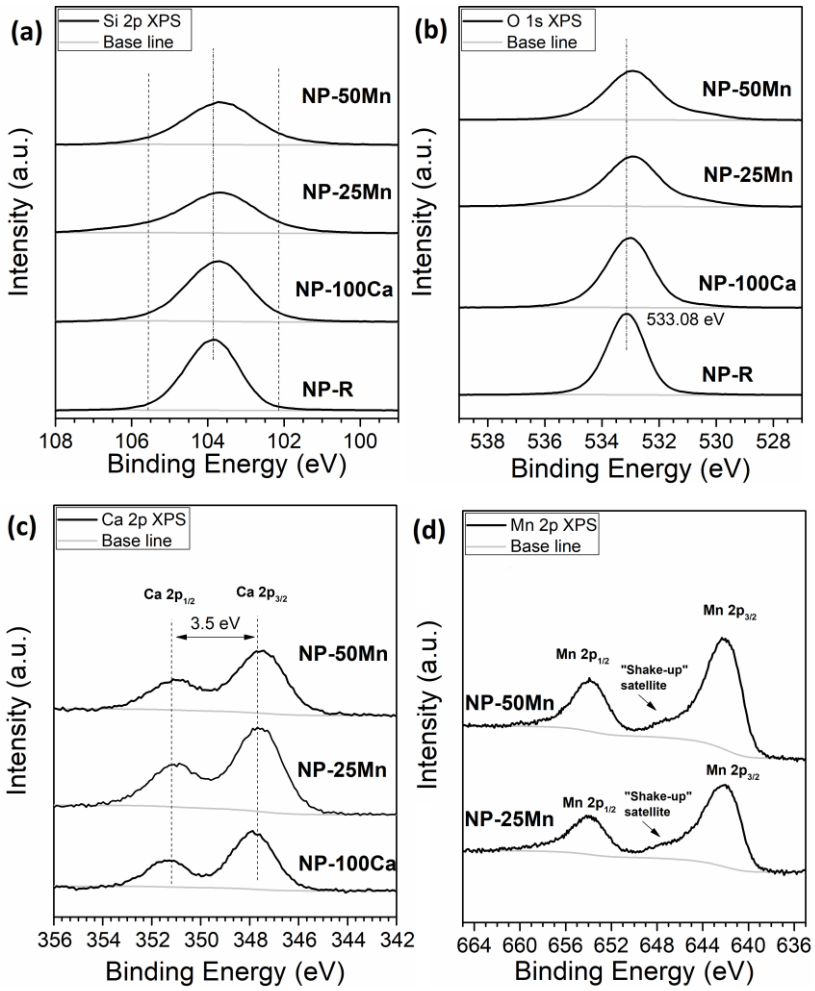

Figure 4: (a) Si 2p, (b) O 1s, (c) Ca 2p and (d) Mn 2p core level XPS spectra of bioactive glass nanoparticles.

^{29}Si MAS NMR allows the identification of Q^n species on the glass network, and it is an important tool for BGs structure evaluation, providing a better understanding of the relationship between the glass structure and properties [36]. Figure 5 presents the ^{29}Si MAS NMR spectra and the calculated percentage of Q^n species is shown in Table 3. The proportion of each species was obtained by the deconvolution of the ^{29}Si MAS-NMR spectra. Results are not shown for NP-50Mn as the higher Mn content affected the ^{29}Si MAS NMR signal, making it difficult to obtain the relative proportion of each species in this sample. In fact, previous works have shown that although the collection and interpretation of NMR data in diamagnetic materials is relatively simple, when paramagnetic ions are present, especially at higher concentrations, the strong electron-nucleus interaction could result in spinning sidebands patterns and a strong line broadening, and even the NMR signal registration becomes problematic [50].

The ^{29}Si MAS NMR data shows that the Si speciation was comprised of a mixture of Q^2, Q^3 and Q^4 species, which exhibit characteristic chemical shifts around -92, -101

and -111 ppm, respectively [51,52]. NP-R presented a high fraction of Q^4 species (87.5 %) and degree of condensation (96.4 %), which indicates a highly interconnected network, in agreement with the previously reported before for silica dense nanoparticles [8]. After the incorporation of calcium and manganese, the degree of condensation reduced for samples NP-100Ca and NP-25Mn, as a result of the increased content of Q^2 and Q^3 species on those samples. The calculated fractions of BO and NBO (shown in Table 3) further confirmed the previously observed results, as a higher degree of BO units is observed for NP-R, and the fraction of NBO units increased after Ca and Mn incorporation, indicative of silica network disruption by the replacement of BO units by NBO.

Results agree with the XPS data that Ca and Mn act as network modifiers in the glass structure, resulting in a reduction on the overall connectivity [8,53]. The slightly higher content of Q^4 units and degree of connectivity for sample NP-25Mn, when compared to NP-100Ca, may be related with the lower amount of network modifiers present in this sample, as not all of the introduced ions were incorporated into the bioactive glass particle structure. Nonetheless, ^{29}Si MAS NMR confirmed the previously observed by the XPS analysis on the role of Ca and Mn in the glass network.

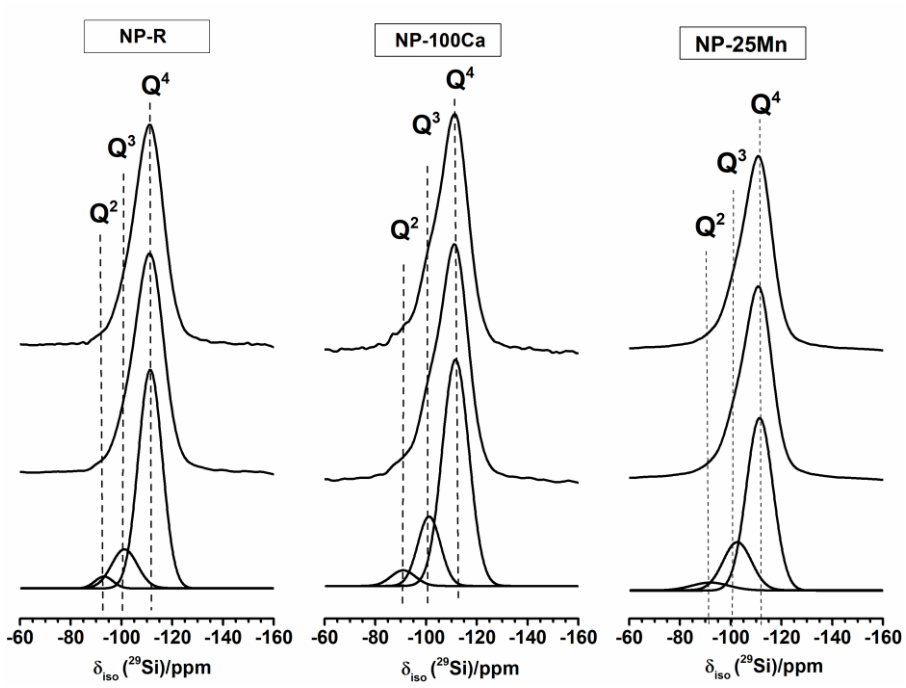

Figure 5: ^{29}Si MAS NMR spectra for bioactive glass samples.

Table 3: Percentage of Q^n species, as determined by ^{29}Si MAS NMR (vr = 5kHz) data, and calculated bridging oxygen (BO) and non-bridging oxygen (NBO) fractions.

Samples	Q^2		Q^3		Q^4		Q^3/Q^4	Dc %	BO	NBO
	δiso [ppm]	I [%]	δiso [ppm]	I [%]	δiso [ppm]	I [%]				
NP-R	-92.1	2.0	-101.2	10.5	-111.4	87.5	0.12	96.4	0.93	0.07
NP-100Ca	-91.0	3.6	-101.2	20.7	-111.6	75.7	0.27	93.0	0.87	0.13
NP-25Mn	-92.0	1.7	-102.6	21.3	-111.4	77.0	0.28	93.8	0.88	0.12

Ion release study

Figure 6 presents the concentration of Si, Ca and Mn in DMEM as measured by ICP-OES. A control sample was also evaluated by incubating DMEM alone, using the same conditions applied for other samples, in which no Si and Mn were detected throughout the study, whereas Ca concentration remained between 61 and 64 ppm. The Si release presented a similar profile for all samples, increasing rapidly during the first 24 h of immersion, reaching up to 35 ppm for NP-R, and stabilizing thereafter. A Si concentration between 37 and 40 ppm was observed after 72 h immersion for all samples. Previous works have shown that silica release could favour biocompatibility [54], and also present stimulatory effects on osteoblasts when released in the range of 0.1 to 100 ppm [55], which is within the release range observed for all samples in this work. The Ca concentration increased sharply during the first 4 h of immersion of the samples containing this ion, stabilizing thereafter. Although NP-100Ca presents the higher Ca content within the glass composition, the DMEM had lower Ca content when compared with NP-25Mn and NP-50Mn, which may be due to the deposition of a calcium phosphate phase on the glass surface [56,57], reducing Ca concentration in solution. However further evaluation should be performed to confirm it. Ca has an important role in the bone mineralization, and could also induce osteoblast proliferation, therefore the Ca release observed in this work could improve the therapeutic effect of the biomaterial [54,58].

A gradual release of Mn was observed for NP-50Mn and NP-25Mn. Previous work showed a concentration-dependent effect of Mn, and concentrations above 0.1 mM, or approximately 5.5 ppm, could inhibit osteoblast proliferation, whereas lower concentrations could present a stimulatory effect [15,18], therefore a controllable ion release is desirable. A maximum Mn concentration of 1.6 ppm was observed after 72 h study, which is below the reported concentration that could impair cell function,

suggesting that the bioactive glass nanoparticles application could maintain the concentration of ions within the therapeutic range. Hence, the dissolution study performed in DMEM indicates that bioactive glass nanoparticles could be used for the sustainable release of different ions within the therapeutic limit, and may represent a promising strategy for "*in situ*" repair of tissues.

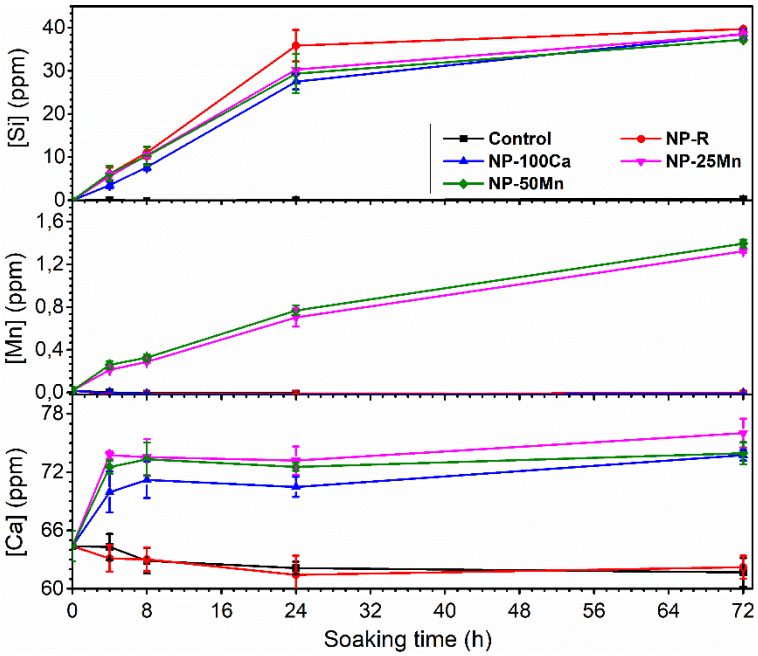

Figure 6: Elemental concentrations in DMEM following immersion of bioactive glass nanoparticles.

In vitro cytotoxicity assay

Human bone marrow-derived stem cells, most commonly referred to as mesenchymal stem cells (hMSCs), are widely applied in cell therapy and tissue engineering strategies and present an important role in tissue regeneration [59]. These cells can be easily isolated and expanded from adult bone marrow aspirates and present a great capacity for pluripotent differentiation into mesenchymal tissues, and when in contact with bioactive glass samples the hMSCs can be stimulated towards osteogenesis [14]. Therefore, hMSCs are relevant for biocompatibility evaluation of biomaterials.

The cell viability of hMSCs exposed to the ionic product of the BGNPs was evaluated by MTT (Figure 7). No cytotoxic effect was observed when hMSCs were exposed for different periods of time to the ionic product of the BGNPs. The exposure to the ionic products of the samples did not significantly alter their mitochondrial metabolic activity when compared to control (untreated cells cultured on TCP), showing high levels of cellular function even in samples containing Mn, not being considered cytotoxic under

the conditions used in this work. Therefore, results show that the manganese incorporation did not alter the bioactive glass cell viability, and the ionic product containing this ion is not cytotoxic.

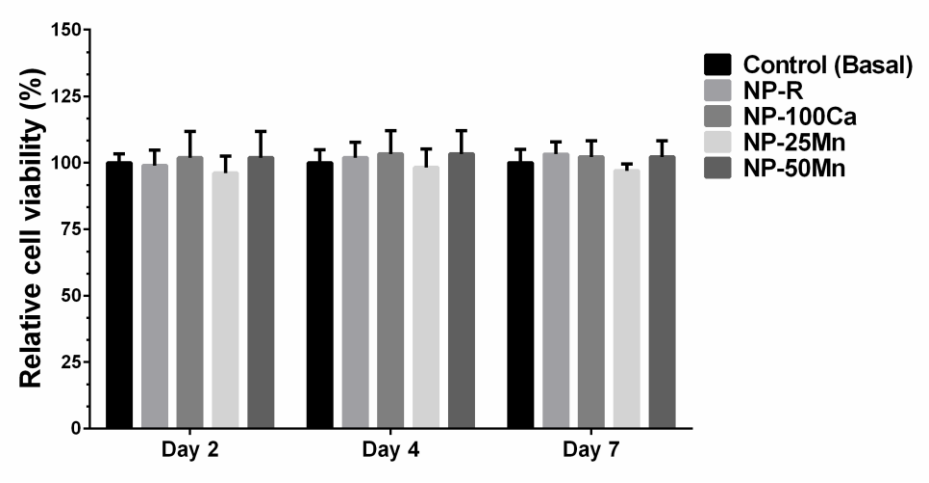

Figure 7: Cell viability of hMSCs exposed to the ionic product of bioactive glass nanoparticles for different periods of time. The data are expressed as mean ± SD of three independent experiments (n = 3).

4 Conclusions

The first spherical bioactive glass nanoparticles containing Mn as a potential therapeutic ion were synthesized and evaluated. Previous work has shown that Mn can influence bone mineralization and that silicate nanoparticles can be vehicles for intracellular delivery of ions. Here, Mn was successfully incorporated into the nanoparticles and effect of Mn content on nanoparticle composition, monosdispersity, structure and ion release was investigated for the SiO_2 – CaO – MnO system. Monodispersed amorphous spherical particles smaller than 150 nm were produced, which is within the reported particle size that can be internalized by cells. Mn incorporation into the glass network was determined through XPS and ^{29}Si MAS-NMR, confirming that Mn played the role of network modifier. Mn release from the particles in DMEM was sustained and no cytotoxic effect was observed on hMSCs exposed to the ionic product of the bioactive glass nanoparticles. The results suggest that the nanoparticles are suitable for intracellular delivery of Mn ions, but future studies are needed to evaluate internalisation of the nanoparticles into a range of cell types.

Acknowledgements

The authors gratefully acknowledge financial support from CNPq, CAPES and FAPEMIG/Brazil and EPSRC for the funding though the CDT in Advanced Characterisation of Materials (CDT-ACM) (EP/L015277/1). The authors also acknowledge EPSRC (EP/M019950/1) for funding and to the Advanced Photoelectron Spectroscopy Laboratory (APSL, Department of Materials, Imperial College London) for XPS analysis. N.L.K. thanks the EPSRC for a PhD studentship through the EPSRC Centre for Doctoral Training in Molecular Analytical Science (EP/L015307/1). J.V.H. thanks the EPSRC, the University of Warwick and the Birmingham Science City Program for partial funding of the solid state NMR infrastructure at Warwick. The latter program accessed the Birmingham Science City Advanced Materials Project 1: Creating and Characterising Next Generation Advanced Materials, which derived support from Advantage West Midlands (AWM) and the European Regional Development Fund (ERDF).

Conflict of interest

The authors declare that there is no personal or financial conflict of interests in the current paper.

5 References

[1] L.L. Hench, R.J. Splinter, W.C. Allen, T.K. Greenlee, Bonding mechanisms at the interface of ceramic prosthetic materials, J. Biomed. Mater. Res. 5 (1971) 117–141. doi:10.1002/jbm.820050611.

[2] L.L. Hench, The story of Bioglass, J. Mater. Sci. Mater. Med. 17 (2006) 967–978. doi:10.1007/s10856-006-0432-z.

[3] J.R. Jones, Review of bioactive glass: From Hench to hybrids, Acta Biomater. 9 (2013) 4457–4486. doi:10.1016/j.actbio.2012.08.023.

[4] S.M. Rabiee, N. Nazparvar, M. Azizian, D. Vashaee, L. Tayebi, Effect of ion substitution on Properties of bioactive glasses: A review, Ceram. Int. 41 (2015) 7241–7251. doi:10.1016/j.ceramint.2015.02.140.

[5] A. Hoppe, N.S. Güldal, A.R. Boccaccini, A review of the biological response to ionic dissolution products from bioactive glasses and glass-ceramics, Biomaterials. 32 (2011) 2757–2774. doi:10.1016/j.biomaterials.2011.01.004.

[6] A. El-Fiqi, T.-H. Kim, M. Kim, M. Eltohamy, J.-E. Won, E.-J. Lee, H.-W. Kim, Capacity of mesoporous bioactive glass nanoparticles to deliver therapeutic molecules, Nanoscale. 4 (2012) 7475. doi:10.1039/c2nr31775c.

[7] P. Naruphontjirakul, A.E. Porter, J.R. Jones, In vitro osteogenesis by intracellular uptake of strontium containing bioactive glass nanoparticles, Acta Biomater. (2017). doi:10.1016/j.actbio.2017.11.008.

[8] S.L. Greasley, S.J. Page, S. Sirovica, S. Chen, R.A. Martin, A. Riveiro, J. V. Hanna, A.E. Porter, J.R. Jones, Controlling particle size in the Stöber process and incorporation of calcium, J. Colloid Interface Sci. 469 (2016) 213–223. doi:10.1016/j.jcis.2016.01.065.

[9] O. Tsigkou, S. Labbaf, M.M. Stevens, A.E. Porter, J.R. Jones, Monodispersed bioactive glass submicron particles and their effect on bone marrow and adipose tissue-derived stem cells, Adv. Healthc. Mater. 3 (2014) 115–125. doi:10.1002/adhm.201300126.

[10] W. Stober, A. Fink, E. Bohn, Controlled growth of monodisperse silica spheres in the micron size range, J. Colloid Interface Sci. 26 (1968) 62–69. http://linkinghub.elsevier.com/retrieve/pii/0021979768902725.

[11] M.-Y. Han, D. Wang, Z. Guo, Y. Han, J. Liang, Z. Teng, W. Yang, Z. Lu, Unraveling the Growth Mechanism of Silica Particles in the Stöber Method: In Situ Seeded Growth Model, Langmuir. 33 (2017) 5879–5890. doi:10.1021/acs.langmuir.7b01140.

[12] P. Naruphontjirakul, S.L. Greasley, S. Chen, A.E. Porter, J.R. Jones, Monodispersed strontium containing bioactive glass nanoparticles and MC3T3-E1 cellular response, Biomed. Glas. 2 (2016) 72–81. doi:10.1515/bglass-2016-0009.

[13] G.M. Luz, J.F. Mano, Preparation and characterization of bioactive glass nanoparticles prepared by sol–gel for biomedical applications, Nanotechnology. 22 (2011) 494014. doi:10.1088/0957-4484/22/49/494014.

[14] S. Labbaf, O. Tsigkou, K.H. Müller, M.M. Stevens, A.E. Porter, J.R. Jones, Spherical bioactive glass particles and their interaction with human mesenchymal stem cells in vitro, Biomaterials. 32 (2011) 1010–1018. doi:10.1016/j.biomaterials.2010.08.082.

[15] F. Lüthen, U. Bulnheim, P.D. Müller, J. Rychly, H. Jesswein, J.G.B. Nebe, Influence of manganese ions on cellular behavior of human osteoblasts in vitro, Biomol. Eng. 24 (2007) 531–536. doi:10.1016/j.bioeng.2007.08.003.

[16] P.M.C. Torres, S.I. Vieira, a. R. Cerqueira, S. Pina, O. a B. Da Cruz Silva, J.C.C. Abrantes, J.M.F. Ferreira, Effects of Mn-doping on the structure and biological properties of β-tricalcium phosphate, J. Inorg. Biochem. 136 (2014) 57–66. doi:10.1016/j.jinorgbio.2014.03.013.

[17] W. Fujitani, Y. Hamada, N. Kawaguchi, S. Mori, K. Daito, A. Uchinaka, T. Matsumoto, Y. Kojima, M. Daito, T. Nakano, N. Matsuura, Synthesis of Hydroxyapatite Containing Manganese and Its Evaluation of Biocompatibility, Nano Biomed. 2 (2010) 37–46. doi:10.11344/nano.2.37.

[18] M. Miola, C.V. Brovarone, G. Maina, F. Rossi, L. Bergandi, D. Ghigo, S. Saracino, M. Maggiora, R.A. Canuto, G. Muzio, E. Vernè, In vitro study of manganese-doped bioactive glasses for bone regeneration, Mater. Sci. Eng. C. 38 (2014) 107–118. doi:10.1016/j.msec.2014.01.045.

[19] Q. Nawaz, M. Atiq, U. Rehman, A. Burkovski, J. Schmidt, A.M. Beltrán, A. Shahid, N.K. Alber, W. Peukert, A.R. Boccaccini, Synthesis and characterization of manganese containing mesoporous bioactive glass nanoparticles for biomedical applications, J. Mater. Sci. Mater. Med. 5 (2018). doi:10.1007/s10856-018-6070-4.

[20] F.E. Ciraldo, E. Boccardi, V. Melli, F. Westhauser, A.R. Boccaccini, Tackling bioactive glass excessive in vitro bioreactivity: Preconditioning approaches for cell culture tests, Acta Biomater. 75 (2018) 3–10. doi:10.1016/j.actbio.2018.05.019.

[21] J. Rouquerol, D. Avnir, C.W. Fairbridge, D.H. Everett, J.M. Haynes, N. Pernicone, J.D.F. Ramsay, K.S.W. Sing, K.K. Unger, Recommendations for the characterization of porous solids (Technical Report), Pure Appl. Chem. 66 (1994) 1739–1758. doi:10.1351/pac199466081739.

[22] K.S.W. Sing, Reporting physisorption data for gas/solid systems with special reference to the determination of surface area and porosity (Recommendations 1984), Pure Appl. Chem. 57 (1985) 603–619. doi:10.1351/pac198557040603.

[23] H.-K. Ting, S. Page, G. Poologasundarampillai, S. Chen, J. V. Hanna, J.R.

Jones, Phosphate content affects structure and bioactivity of sol-gel silicate bioactive glasses, Int. J. Appl. Glas. Sci. (2017). doi:10.1111/ijag.12322.

[24] H.W. Nesbitt, G.M. Bancroft, G.S. Henderson, R. Ho, K.N. Dalby, Y. Huang, Z. Yan, Bridging, non-bridging and free (O2–) oxygen in Na2O-SiO2 glasses: An X-ray Photoelectron Spectroscopic (XPS) and Nuclear Magnetic Resonance (NMR) study, J. Non. Cryst. Solids. 357 (2011) 170–180. doi:10.1016/j.jnoncrysol.2010.09.031.

[25] S. Li, A.L. Maçon, M. Jacquemin, M.M. Stevens, J.R. Jones, Sol–gel derived lithium-releasing glass for cartilage regeneration, J. Biomater. Appl. 32 (2017) 104–113. doi:10.1177/0885328217706640.

[26] B. Yu, C. a Turdean-Ionescu, R. a Martin, R.J. Newport, J. V Hanna, M.E. Smith, J.R. Jones, Effect of Calcium Source on Structure and Properties of Sol–Gel Derived Bioactive Glasses, Langmuir. 28 (2012) 17465–17476. doi:10.1021/la303768b.

[27] A.A.R. de Oliveira, D.A. de Souza, L.L.S. Dias, S.M. de Carvalho, H.S. Mansur, M. de Magalhães Pereira, Synthesis, characterization and cytocompatibility of spherical bioactive glass nanoparticles for potential hard tissue engineering applications, Biomed. Mater. 8 (2013) 025011. doi:10.1088/1748-6041/8/2/025011.

[28] A. Doostmohammadi, A. Monshi, R. Salehi, M.H. Fathi, Z. Golniya, A.U. Daniels, Bioactive glass nanoparticles with negative zeta potential, Ceram. Int. 37 (2011) 2311–2316. doi:10.1016/j.ceramint.2011.03.026.

[29] S. Honary, F. Zahir, Effect of Zeta Potential on the Properties of Nano - Drug Delivery Systems - A Review (Part 2), Trop. J. Pharm. Al Res. 12 (2013) 265–273. doi:10.4314/tjpr.v12i2.19.

[30] A. Lukowiak, J. Lao, J. Lacroix, J.-M. Nedelec, Bioactive glass nanoparticles obtained through sol–gel chemistry, Chem. Commun. 49 (2013) 6620. doi:10.1039/c3cc00003f.

[31] A.M. El-Kady, A.F. Ali, Fabrication and characterization of ZnO modified bioactive glass nanoparticles, Ceram. Int. 38 (2012) 1195–1204. doi:10.1016/j.ceramint.2011.07.069.

[32] J. Serra, P. González, S. Liste, C. Serra, S. Chiussi, B. León, M. Pérez-Amor, H.O. Ylänen, M. Hupa, FTIR and XPS studies of bioactive silica based glasses, J. Non. Cryst. Solids. 332 (2003) 20–27. doi:10.1016/j.jnoncrysol.2003.09.013.

[33] G.M. Luz, J.F. Mano, Preparation and characterization of bioactive glass nanoparticles prepared by sol–gel for biomedical applications, Nanotechnology. 22 (2011) 494014. doi:10.1088/0957-4484/22/49/494014.

[34] H. Pirayesh, J. a. Nychka, Sol-gel synthesis of bioactive glass-ceramic 45S5 and its in vitro dissolution and mineralization behavior, J. Am. Ceram. Soc. 96 (2013) 1643–1650. doi:10.1111/jace.12190.

[35] K.N. Dalby, H.W. Nesbitt, V.P. Zakaznova-Herzog, P.L. King, Resolution of bridging oxygen signals from O 1s spectra of silicate glasses using XPS: Implications for O and Si speciation, Geochim. Cosmochim. Acta. 71 (2007) 4297–4313. doi:10.1016/j.gca.2007.07.005.

[36] S. Shruti, A.J. Salinas, G. Malavasi, G. Lusvardi, L. Menabue, C. Ferrara, P. Mustarelli, M. Vallet-Regì, Structural and in vitro study of cerium, gallium and zinc containing sol–gel bioactive glasses, J. Mater. Chem. 22 (2012) 13698–13706. doi:10.1039/c2jm31767b.

[37] A. Mekki, M. Salim, XPS study of transition metal doped silicate glasses, J. Electron Spectros. Relat. Phenomena. 101 (1999) 227–232. doi:10.1016/S0368-2048(98)00450-2.

[38] E. Verné, O. Bretcanu, C. Balagna, C.L. Bianchi, M. Cannas, S. Gatti, C. Vitale-Brovarone, Early stage reactivity and in vitro behavior of silica-based bioactive glasses and glass-ceramics, J. Mater. Sci. Mater. Med. 20 (2009) 75–87. doi:10.1007/s10856-008-3537-8.

[39] B. Roy, H. Jain, S.K. Saha, D. Chakravorty, Comparison of structure of alkali silicate glasses prepared by sol-gel and melt-quench methods, J. Non. Cryst. Solids. 183 (1995) 268–276. doi:10.1016/0022-3093(94)00633-4.

[40] H. Shin, J. Jung, S. Kim, W. Lee, XPS Analysis on Chemical Properties of Calcium Phosphate Thin Films and Osteoblastic HOS Cell Responses, J Ind Eng Chem. 12 (2006) 476–483.

[41] M. Ni, B.D. Ratner, Differentiation of Calcium Carbonate Polymorphs by Surface

Analysis Technique - An XPS and TOF-SIMS study, Natl. Institue Heal. 40 (2014) 1356–1361. doi:10.1002/sia.2904.Differentiation.

[42] B. Demri, D. Muster, XPS study of some calcium compounds, J. Mater. Process. Technol. 55 (1995) 311–314. doi:10.1016/0924-0136(95)02023-3.

[43] H.W. Nesbitt, D. Banerjee, Interpretation of XPS Mn(2p) spectra of Mn oxyhydroxides and constraints on the mechanism of MnO2 precipitation, Am. Mineral. 83 (1998) 305–315. doi:10.2138/am-1998-3-414.

[44] R. Gostynski, J. Conradie, E. Erasmus, Significance of the electron-density of molecular fragments on the properties of manganese(iii) β-diketonato complexes: an XPS and DFT study, RSC Adv. 7 (2017) 27718–27728. doi:10.1039/C7RA04921H.

[45] M.C. Biesinger, B.P. Payne, A.P. Grosvenor, L.W.M. Lau, A.R. Gerson, R.S.C. Smart, Resolving surface chemical states in XPS analysis of first row transition metals, oxides and hydroxides: Cr, Mn, Fe, Co and Ni, Appl. Surf. Sci. 257 (2011) 2717–2730. doi:10.1016/j.apsusc.2010.10.051.

[46] J.M. Cerrato, M.F. Hochella, W.R. Knocke, A.M. Dietrich, T.F. Cromer, Use of XPS to identify the oxidation state of Mn in solid surfaces of filtration media oxide samples from drinking water treatment plants, Environ. Sci. Technol. 44 (2010) 5881–5886. doi:10.1021/es100547q.

[47] C. Poinsignon, G. Berthomé, B. Prélot, F. Thomas, F. Villiéras, Manganese Dioxides Surface Properties Studied by XPS and Gas Adsorption, J. Electrochem. Soc. 151 (2004) A1611–A1616. doi:10.1149/1.1789411.

[48] O.A. Bulavchenko, Z.S. Vinokurov, T.N. Afonasenko, P.G. Tsyrul'nikov, S. V Tsybulya, A.A. Saraev, V. V Kaichev, Reduction of mixed Mn-Zr oxides: in situ XPS and XRD studies, Dalt. Trans. 44 (2015) 15499–15507. doi:10.1039/C5DT01440A.

[49] P. Pascuta, G. Borodi, N. Jumate, I. Vida-Simiti, D. Viorel, E. Culea, The structural role of manganese ions in some zinc phosphate glasses and glass ceramics, J. Alloys Compd. 504 (2010) 479–483. doi:10.1016/j.jallcom.2010.05.147.

[50] V.I. Bakhmutov, B.G. Shpeizer, A. Clearfield, Solid-state NMR spectra of

paramagnetic silica-based materials: observation of29Si and27Al nuclei in the first coordination spheres of manganese ions, Magn. Reson. Chem. 44 (2006) 861–867. doi:10.1002/mrc.1866.

[51] G. Poologasundarampillai, D. Wang, S. Li, J. Nakamura, R. Bradley, P.D. Lee, M.M. Stevens, D.S. McPhail, T. Kasuga, J.R. Jones, Cotton-wool-like bioactive glasses for bone regeneration., Acta Biomater. 10 (2014) 3733–46. doi:10.1016/j.actbio.2014.05.020.

[52] Z. Lin, J.R. Jones, J. V Hanna, M. Smith, A multinuclear solid state NMR spectroscopic study of the structural evolution of disordered calcium silicate sol-gel biomaterials, Phys. Chem. Chem. Phys. 17 (2015) 2540–9. doi:10.1039/c4cp04492d.

[53] A.L.B. Maçon, M. Jacquemin, S.J. Page, S. Li, S. Bertazzo, M.M. Stevens, J. V. Hanna, J.R. Jones, Lithium-silicate sol–gel bioactive glass and the effect of lithium precursor on structure–property relationships, J. Sol-Gel Sci. Technol. (2016). doi:10.1007/s10971-016-4097-x.

[54] A. Goel, R.R. Rajagopal, J.M.F. Ferreira, Influence of strontium on structure, sintering and biodegradation behaviour of CaO-MgO-SrO-SiO2-P2O5-CaF2 glasses, Acta Biomater. 7 (2011) 4071–4080. doi:10.1016/j.actbio.2011.06.047.

[55] I. Christodoulou, L.D.K. Buttery, P. Saravanapavan, G. Tai, L.L. Hench, J.M. Polak, Dose- and time-dependent effect of bioactive gel-glass ionic-dissolution products on human fetal osteoblast-specific gene expression, J. Biomed. Mater. Res. - Part B Appl. Biomater. 74 (2005) 529–537. doi:10.1002/jbm.b.30249.

[56] D.C. Clupper, J.E. Gough, M.M. Hall, A.G. Clare, W.C. Lacourse, L.L. Hench, In vitro bioactivity of S520 glass fibers and initial assessment of osteoblast attachment, (2003).

[57] D. Rohanová, A.R. Boccaccini, D. Horkavcov, P. Bozdechová, P. Bezdicka, M. Castorálová, Is non-buffered DMEM solution a suitable medium for in vitro bioactivity tests ?, J. Mater. Chem. B. 2 (2014) 5068–5076. doi:10.1039/c4tb00187g.

[58] S. Murphy, D. Boyd, S. Moane, M. Bennett, The effect of composition on ion release from Ca-Sr-Na-Zn-Si glass bone grafts, J. Mater. Sci. Mater. Med. 20 (2009) 2207–2214. doi:10.1007/s10856-009-3789-y.

[59] M.M. Azevedo, O. Tsigkou, R. Nair, J.R. Jones, G. Jell, M.M. Stevens, Hypoxia Inducible Factor-Stabilizing Bioactive Glasses for Directing Mesenchymal Stem Cell Behavior., Tissue Eng. Part A. 00 (2014) 1–8. doi:10.1089/ten.TEA.2014.0083.